Sensors and Actuators A 331 (2021) 112979

Contents lists available at ScienceDirect

Sensors and Actuators A: Physical

journal homepage: www.elsevier.com/locate/sna

Measurement of the positions of light sensors on a mobile frame being tracked with a lighthouse localization system

A.F.M. Paijens[a,b], L. Huang[a,b,*], A.M. Al-Jumaily[a,b]

[a] School of Engineering, Computer and Mathematical Sciences, New Zealand
[b] Auckland University of Technology, Auckland, New Zealand

ARTICLE INFO

Article history:
Received 17 February 2021
Received in revised form 9 July 2021
Accepted 12 July 2021
Available online 21 July 2021

Keywords:
Localization
Lighthouse
Light sensor
Time measurement
Sensor position
Perspective projection
Conics
Camera calibration

ABSTRACT

The laser lighthouse is a nearly 40 year old concept that only recently had a practical incarnation in the HTC Vive VR kit base station, a single beacon that sweeps a light sheet at a fixed frequency like a lighthouse. It can be placed on a flat surface in any position from where it has a line of sight to a mobile frame equipped with light sensors and some computing power to record and process time stamps at the passage of the light sheet. From the recorded timestamp and the positions of the sensors in the mobile frame, the position of the frame in the (global) coordinate frame of the lighthouse can be established. Surface applicable light sensors have been announced for this purpose, that can turn any object into a trackable object with the laser lighthouse system. The accuracy of the positions of the sensors in the mobile frame is cardinal to the accuracy of the calculated position of the mobile frame. This presents a challenge as the positions of sensors on the surface of an object are not easy to obtain in a 3D coordinate frame. Even if they are available in a CAD design, manufacturing tolerances might cause the positions of the sensors to deviate from their designed positions. In this first paper on this subject, a method is proposed to measure the position of the sensors in the mobile frame using (hand-) measurement of the distance between a small number of designated features of the mobile frame only. The positions of the light sensors in the mobile frame are derived from the timestamps recorded by the light sensors in a procedure that subjects the mobile frame to constrained rotations. The efficacy of the proposed method is tested and validated experimentally. The sensor positions obtained with the method improve the accuracy of the localization of the mobile frame.

1. Introduction

In 2015 HTC introduces the Vive virtual reality gaming kit, that uses a lighthouse concept to offer 3D localization technology for Virtual Reality gamers in the consumer market. It is not the first lighthouse system introduced [1–3], but it is the first consumer electronics system that works well. For this reason it is quite popular amongst researchers in robotics and computer vision. The laser lighthouse features a single beacon in stationary position, spinning a light sheet around one or multiple axes, with a fixed frequency similar to that of a lighthouse. A tracked frame is equipped with a minimum of three light sensors in different positions with which a time stamp is recorded by each sensor when it is struck by the passing light sheet. In addition, the lighthouse also emits a synchronization signal to indicate when the light sheet passes through a fixed orientation in the rotation, as a start signal for the subsequent period. From the recorded time stamps and the speed of rotation of the lighthouse, angles of incidence of the light sheet at the sensors can be established and used to calculate the position of the frame relative to the lighthouse. If the lighthouse sweeps a single light sheet, this is a planar position in the sweeping plane [4]. If the lighthouse sweeps multiple light sheets in different planes, a spatial 3D position can be obtained. Compared to other localization systems using triangulation based on multiple beacons, the laser lighthouse concept is a wonder of simplicity. For a single lighthouse there is no need for calibration of the position of the beacons relative to each other, or synchronization of the signals emitted by different beacons. A single lighthouse can be positioned in a convenient place and will localize the tracked frame as long as a line of sight is maintained. The low requirements of the lighthouse system to the conditioning of the workspace makes it an attractive solution to support field deployment of mobile frames

* Corresponding author at: Auckland University of Technology, Auckland, New Zealand.
E-mail addresses: antonius.paijens@aut.ac.nz (A.F.M. Paijens), loulin.huang@aut.ac.nz (L. Huang), ahmed.aljumaily@aut.ac.nz (A.M. Al-Jumaily).

https://doi.org/10.1016/j.sna.2021.112979
0924-4247/

like mobile robots. The secret of the Vive system are the application of hard disk drive motors to spin the laser beams resulting in highly accurate timings of the sweeps. Impromptu tests with the set using two lighthouses, reportedly demonstrate a positioning resolution of 0.3 mm in a workspace of 5 m by 5 m. This makes the lighthouse system a viable solution to localize and position robots in manufacturing operations for example. The system is designed for VR applications however and HTC has not published details of the algorithms used to establish the position of the objects tracked. The developer of the system acknowledged a video on the working principle and presented the concepts on its workings on the Hackaday Supercon 2016. Although several researchers have reported on the accuracy of poses obtained with the HTC VR-kit, comparison of the figures presented is difficult as the conditions at which the results have been obtained are very different. Greiff et al. research the performance of the multiple Vive system base stations to locate micro unmanned aerial vehicles (MUAVs) in a 3 m cubical operating range and find millimeter range localization accuracy [5]. Kilberg et al. reports errors of a few centimeters using one lighthouse with their own tracker within a 1 meter working range [6]. Niehorster et al. find deviations of the same centimeter order of magnitude while operating two lighthouses to locate a tracker in an operating range of 5 m diagonal [7]. Jansen et al. measure the position and orientation of two stationary lighthouse base stations separated by a distance between 1 and 4 m, relative to each other [8]. They use their own tracker at a distance between 2 and 6 m from the lighthouses and report a positional accuracy just below 1 cm. Sletten observes resolution at millimeter scale in his experiments [9].

The positions of the sensors on the frame tracked are cardinal in its localization with a lighthouse, but this aspect has not received attention in the research community yet. Kits with surface applicable sensors have been announced to make existing objects trackable, leaving the user with the challenge to find the coordinates of the sensors' positions after application. This paper intends to provide some handles to find them, derived from camera calibration methods. Section 2 elaborates the operation of a lighthouse and Section 3 explains the fundamentals of retrieving a position from it. Section 4 quantifies the propagation of errors in the position of a sensor into an error in the calculated location of the mobile frame. To minimize errors in sensor positions, a camera calibration method is introduced in Section 5 with application to the lighthouse. The method is demonstrated with some experiments in Section 6, validated in Section 7 and concluded in Section 8.

2. Operation of the HTC Vive lighthouse

The lighthouse used for the research described in this paper is one of two "base stations", version 1.0 included in the HTC Vive Virtual Reality (VR) kit. Its operation is illustrated in Fig. 1. The box shaped "base station" emits two laser beams at the negative ${}^{C}z$ side of the local coordinate system C of the box. The two beams are spread into a light sheet with a viewing range of $2/3\pi$ rad. each.

Light sheet "h" rotates around a horizontal ${}^{C}x$-axis perpendicular to the ${}^{C}y$–${}^{C}z$ plane and sheet "v" around the vertical ${}^{C}y$-axis perpendicular the ${}^{C}x$–${}^{C}z$ plane, as indicated in Fig. 1. The origin of the coordinate system of the lighthouse ${}^{C}0$, which coincides with the intersection of the rotation axes of the sheets, is not located exactly in the center of the base station as might be suggested in Fig. 1. Both light sheets spin in positive direction around their axis of rotation at a frequency of 60 Hz corresponding to an angular velocity of $\omega = 120\pi$ rad/s. The phases of sheet "h" and "v" are shifted by π rad., causing them to swipe alternately through the space at the negative z-side of the lighthouse. Intersection of the light sheets as drawn in Fig. 1 for illustration purposes, does not occur in practice. In addition to the light sheets, the base station emits omnidirectional light pulses for synchronization when either light sheet passes through a fixed orientation in their sweeping motion. A sync pulse is emitted upon light sheet "h" passing through the negative y-axis and a upon light sheet "v" passing through the x-axis. At a rotation frequency of 60 Hz for both sheets, the start time of the sync pulses are exactly $1/60 \times 1/2 = 8.333$ ms apart and mark the "heartbeat" of the lighthouse. The duration of the sync pulses varies between 62.5 and 135 μs which encodes three bit states that identify:

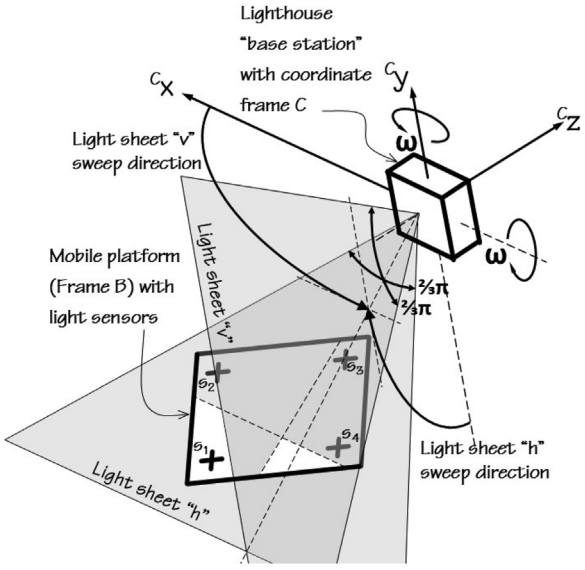

Fig. 1. Sweeping of light sheets by the lighthouse.

1. the status of the sweep of the second base station; for the research in this paper only one base station will be used, hence the status of this bit is always 0;
2. the light sheet that starts its sweep ("h" or "v");
3. one bit of a sequence broadcasted by the base station, encoding status information.

The mobile frame to be localized by the lighthouse is represented by Frame B in Fig. 1. It is equipped with multiple light sensors $s_i (i = 1, 2, 3, \ldots)$ to capture the sweeps of the light sheets emitted by the lighthouse. The sequence of light pulses as observed by a light sensor $s_i (i = 1, 2, 3, \ldots)$ exposed to the lighthouse is depicted in Fig. 2. The heartbeat of the base station can be filtered out by the edges 8.33 ms apart. The start of a sync pulse as observed by the rising edge of a heartbeat at all light sensors marks the beginning of a new sweep period n_t and is time-stamped $t_0(n_t)$, $(n_t \in \mathbb{N})$. The timing of the first falling edge designates the end of the sync pulse and allows for decoding of the 3 bit code, identifying whether the light sheet coming up is "h"or "v". The subsequent rising and falling edges mark the passing of the light sheet over the sensor. For the purpose of position measurement, the median time between the rising and falling edge is taken as the "time of strike" of the sensor by the light sheet in period n_t. This time is indicated as $t_l(n_t)$ in the table in Fig. 2. The subsequent rising edge marks the end of the period of the current sweep n_t and the start of the sync pulse for the alternate "v" sweep $n_t + 1$, in which again the time of strike $t_l(n_t + 1)$ is measured. Fig. 2 is not drawn to scale as in practice the duration of the sync pulses is typically more than one order of magnitude longer than the sensor strikes.

Since t_0 is defined by the passing of the light sheet through a fixed orientation, the time of strike t_l allows for calculation of the position of the light sheet at which the strike takes place. The posi-

Period	n_t	n_t+1	n_t+2	n_t+3
Sweep	h	v	h	v
Δt	$\Delta t_h(n_t) = t_l(n_t) - t_0(n_t)$	$\Delta t_v(n_t+1)=t_l(n_t+1)-t_0(n_t+1)$	$\Delta t_h(n_t+2)=t_l(n_t+2)-t_0(n_t+2)$	$\Delta t_v(n_t+3)=t_l(n_t+3)-t_0(n_t+3)$
Φ(n)	$\Phi(n_t) = \omega\,\Delta t_h(n_t) - ½\pi$	-	$\Phi(n_t+2)=\omega\,\Delta t_h(n_t+2)-½\pi$	-
Θ(n)	-	$\Theta(n_t+1)=\omega\,\Delta t_v(n_t+1)-½\pi$	-	$\Theta(n_t+3)=\omega\,\Delta t_v(n_t+3)-½\pi$

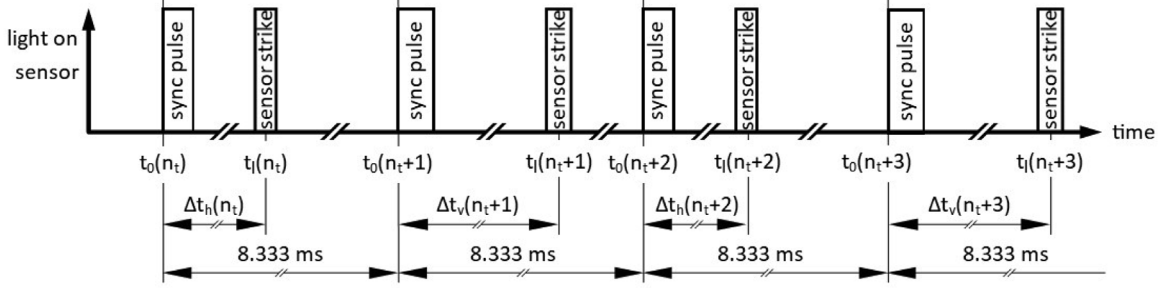

Fig. 2. Light pulses observed by a light sensor in exposure range of the lighthouse.

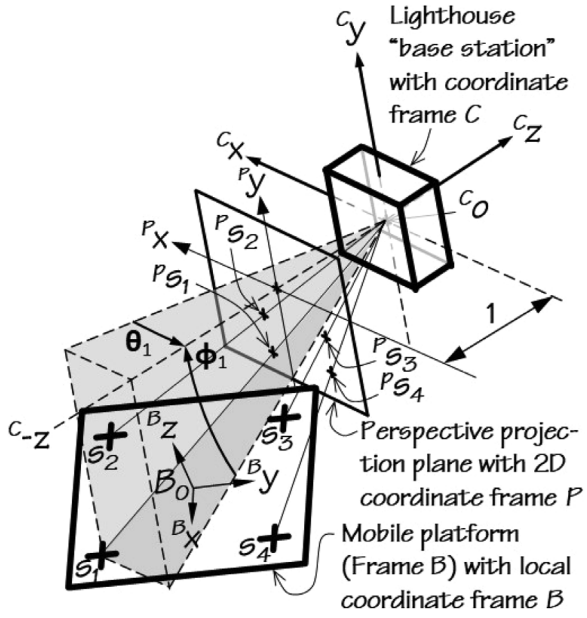

Fig. 3. Positions of light sensors $s_i (i = 1, 2, 3, \ldots)$ in coordinate systems of the mobile frame and the lighthouse and in perspective projection.

tions are expressed through angles $\phi(n_t)$ and $\theta(n_t)$ for sheets "h" and "v" respectively as defined in the table in Fig. 2 and illustrated in Fig. 3:

$$\phi(n_t) = \omega(t_l(n_t) - t_0(n_t)) - \frac{1}{2}\pi$$

$$\theta(n_t) = \omega(t_l(n_t) - t_0(n_t)) - \frac{1}{2}\pi$$

The expressions include an offset $-\frac{1}{2}\pi$ for both angles ϕ and θ, to align the orientations $\phi = 0$ and $\theta = 0$ of the light sheets with the negative z-axis, normal to front face of the base station.

As the analysis in this paper applies to any sweep period of the lighthouse, the reference to a particular time frame (n_t) is dropped in the notation.

3. Position measurement with a lighthouse

With the setup in place to measure angles ϕ_i and θ_i for all sensors $s_i (i = 1, 2, 3, \ldots)$, the position of the mobile frame in the lighthouse coordinate Frame C can be established through the geometrical relationship between the angles and the perspective projection of the sensors:

$${}^P s_i{}^T = [{}^P x_i \; {}^P y_i] = \left[\frac{{}^C x_i}{{}^C z_i} \; \frac{{}^C y_i}{{}^C z_i}\right] = [\tan(\theta_i) \; \tan(\phi_i)] \tag{1}$$

The ${}^C z_i$ coordinate cannot be established from the angles measured by the lighthouse system for a single sensor. To estimate ${}^C z_i$, sounding angles from the lighthouse are required for at least three sensors of which the positions ${}^B s_i^T = [{}^B x_i \; {}^B y_i \; {}^B z_i]$ in Frame B are known. Islam et al. present a trigonometric solution for this purpose, where the angle ϕ as measured with a lighthouse setup, is interpreted as the elevation (polar) angle in spherical coordinates [3]. This seems incorrect however, as Jansen et al. indicate that ϕ is not the spherical elevation angle, but the projection of the spherical elevation angle on the ${}^C y$–${}^C z$ plane (as used in this paper) [8].

Borges et al. and Jansen et al. reconstruct the pose of Frame B by minimization of the difference between the angles at which the sensors are sounded by the lighthouse and the corresponding angles calculated from the body pose, using Expression (1) [10,8]. The body pose is specified by a rotation matrix R and translation vector T of Frame B corresponding to its orientation and position relative to Frame C. Formulating this as a space transformation of the sensors positions ${}^B s_i$ in homogeneous coordinates, the minimization can be expressed as estimating R, T and ${}^C z_i$ from the following equation for all sensors s_i on Frame B:

$${}^C s_i = \begin{bmatrix} {}^C x_i \\ {}^C y_i \\ {}^C z_i \end{bmatrix} = \begin{bmatrix} R|T \end{bmatrix} \begin{bmatrix} {}^B s_i \\ 1 \end{bmatrix} \tag{2}$$

Eq. (2) defines three relationships between ${}^C s_i = [{}^C x_i \; {}^C y_i \; {}^C z_i]$ and ${}^B s_i = [{}^B x_i \; {}^B y_i \; {}^B z_i]$ for each sensor with which the 6 degrees of freedom represented by R and T have to be estimated, together with ${}^C z_i$. Since R and T are identical for each sensor mounted on the same rigid body, additional sensors only add an unknown ${}^C z_i$ to the sys-

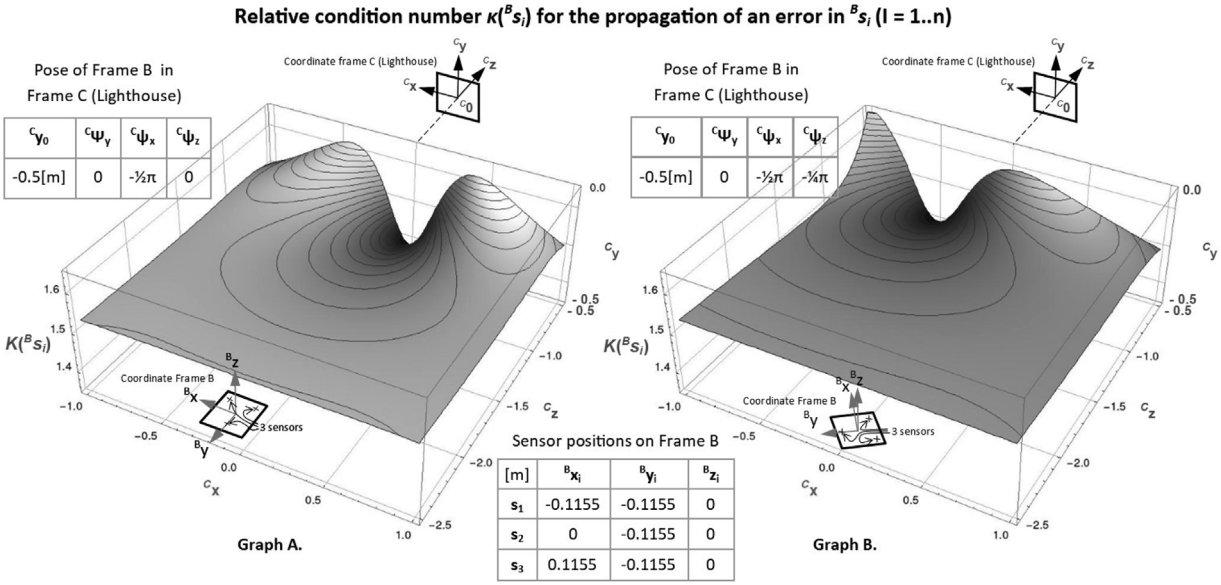

Pose of Frame B in Frame C (Lighthouse)			
${}^{C}y_0$	${}^{C}\psi_y$	${}^{C}\psi_x$	${}^{C}\psi_z$
-0.5[m]	0	-½π	0

Pose of Frame B in Frame C (Lighthouse)			
${}^{C}y_0$	${}^{C}\psi_y$	${}^{C}\psi_x$	${}^{C}\psi_z$
-0.5[m]	0	-½π	-¼π

Sensor positions on Frame B			
[m]	${}^{B}x_i$	${}^{B}y_i$	${}^{B}z_i$
s_1	-0.1155	-0.1155	0
s_2	0	-0.1155	0
s_3	0.1155	-0.1155	0

Fig. 4. Propagation of an error in the sensor position ${}^{B}s$ into the computed position of Frame B in Frame C, expressed in a relative condition number $\kappa({}^{B}s_i)$, for two values of ${}^{C}\psi_z$.

tem of equations. This implies that with a minimum of three sensors on Frame B, a system of nine equations is defined with which R, T and ${}^{C}z_i$ can be estimated and the position of Frame B in Frame C established.

4. Error propagation in the lighthouse position measurement

In this section it is assumed that the position of Frame B in Frame C will be determined with the minimum number of three sensors, identified as s_p, s_q and s_r. Obviously, the positions of these sensors in Frame B are cardinal parameters in the calculation of the mobile frame position. Although the position of each sensor will generally be established as part of the design process of the rigid (frame) body, it will be subjected to tolerances of manufacturing and assembly tolerances on the physical frame. The introduction of surface applicable sensors will make the requirement for determination of the sensor positions obvious. Measuring the positions directly can be challenging as a consequence of their placement. Moreover, the light sensors used in the present research have a radiant sensitive area of 7.5 mm^2, of which a "focal point" representative for the timing of detection of the light sheet has to be established. It seems sensible to use the geometric center of the sensor surface for this purpose, but without measurement of the sensor position this remains a "best guess".

To estimate the sensors' position error $\Delta^{C}s_i$ in Frame C from their error $\Delta^{B}s_i$ in Frame B, a relative conditions number $\kappa({}^{B}s_i)$, which gives the ratio between the relative errors $\Delta^{C}s_i/{}^{C}s_i$ and $\Delta^{B}s/{}^{B}s$, $i \in (p, q, r)$, is needed [11]. $\kappa({}^{B}s_i)$ is derived from the relationship between ${}^{C}s$ and ${}^{B}s$, through:

$$\kappa({}^{B}s_i) = \frac{\|{}^{B}s_i\| \|J({}^{C}s_i, {}^{B}s_i)\|}{\|{}^{C}s_i\|}, \quad i \in (p, q, r) \tag{3}$$

where the Jacobian $J({}^{C}s_i, {}^{B}s_i)$ is the differentiation of ${}^{C}s_i$ with respect to ${}^{B}s_i$.

${}^{C}s_i$ is solved for three sensors s_p, s_q and s_r simultaneously in two steps.

Firstly the parameters for $R = R({}^{C}\psi)$ and T are estimated, establishing the pose of Frame B in Frame C. ${}^{C}\psi$ comprises the Euler angles ${}^{C}\psi^T = [{}^{C}\psi_x\ {}^{C}\psi_y\ {}^{C}\psi_z]$ of rotational angles around subsequently the y, x and z axes of Frame C and $R = R_z({}^{C}\psi_z)\, R_x({}^{C}\psi_x)\, R_y({}^{C}\psi_y)$. T equals the position of the origin of Frame B in Frame C: $T^T = {}^{C}B_o^T = [{}^{C}x_B\ {}^{C}y_B\ {}^{C}z_B]$. ${}^{C}\psi$ and ${}^{C}B_o$ are approximated using the Levenberg–Marquardt algorithm [12] until the positions of the sensors in Frame C as computed with Eq. (2) match the angles ϕ_p, ϕ_q, ϕ_r and $\theta_p, \theta_q, \theta_r$ at which the three sensors are sounded by the lighthouse system:

$$({}^{\tilde{C}}\psi, {}^{\tilde{C}}B_o, {}^{\tilde{C}}z_i) = arg \min_{({}^{C}\psi, {}^{C}B_o, {}^{C}z_i)} \left[\sum_{i=(p,q,r)} \left(\begin{bmatrix} {}^{C}x_i/{}^{C}z_i \\ {}^{C}y_i/{}^{C}z_i \end{bmatrix} - \begin{bmatrix} \tan(\theta_i) \\ \tan(\phi_i) \end{bmatrix} \right)^2 \right]$$

Next, estimates for ${}^{C}s_p$, ${}^{C}s_q$ and ${}^{C}s_r$ are calculated with Eq. (2) using the estimated values ${}^{\tilde{C}}\psi$, ${}^{\tilde{C}}B_o$ and ${}^{\tilde{C}}z_i$.

Since the values of ${}^{B}s$ are used to find the estimates for ${}^{C}\psi$ and ${}^{C}B_o$, the latter are (implicit) functions of ${}^{B}s$: ${}^{C}\psi = {}^{C}\psi({}^{B}s)$, ${}^{C}B_o = {}^{C}B_o({}^{B}s)$. As a consequence $J({}^{C}s, {}^{B}s)$ has to be evaluated as:

$$J({}^{C}s, {}^{B}s) = \left[\frac{\partial {}^{C}s}{\partial {}^{C}\psi} \frac{\partial {}^{C}\psi}{\partial {}^{B}s} + \frac{\partial {}^{C}s}{\partial {}^{C}B_0} \frac{\partial {}^{C}B_0}{\partial {}^{B}s} + \frac{\partial {}^{C}s}{\partial {}^{B}s} \right] \tag{4}$$

The differential quotients $\partial {}^{C}\psi / \partial {}^{B}s_i$ and $\partial {}^{C}B_0 / \partial {}^{B}s_i$ can be derived from implicit differentiation of Eq. (1) to ${}^{B}s_i$ for $i \in (p, q, r)$, in which the terms $tan(\phi_i)$ and $tan(\theta_i)$ are constant as they refer to one measurement sample for θ_i and ϕ_i only. This reflects the actual situation in which measured values from one sweep of the lighthouse in both sweeping planes are plugged into θ_i and ϕ_i to compute ${}^{C}\psi$ and ${}^{C}B_o$:

$$\frac{\partial}{\partial {}^{B}s} [\tan(\theta_i)\ \tan(\phi_i)] = [0\ 0] \tag{5}$$

In the relation between ${}^{C}\psi$ and ${}^{C}B_o$, it is assumed that the values for θ_i and ϕ_i are acquired with Frame B being in exactly the same position in Frame C. Hence Frame B does not move in the time interval between the timestamps of the sensors involved.

The differential quotients $\partial {}^{C}\psi / \partial {}^{B}s_i$ and $\partial {}^{C}B_0 / \partial {}^{B}s_i$ are elaborated in Appendix A.

Inserting the resulting expressions in Eq. (3) allows calculation of $\kappa({}^{B}s_i)$ as a function of ${}^{C}\psi$ and ${}^{C}B_0$. Fig. 4 presents two graphs of this function, for the intended application scenario of a lighthouse system: $\kappa({}^{B}s_i)$ is computed over a planar space of 2 m by 2 m, with the lighthouse positioned at a height of 1 m over and at 0.5 m off the side of this space. In Graph A the ${}^{B}x$, ${}^{B}y$ and ${}^{B}z$ axes of Frame B

(the mobile frame) are aligned with the ${}^{C}x$, ${}^{C}z$ and ${}^{C}y$ axes of Frame C (the lighthouse) respectively. In Graph B, Frame B is offset over an angle of $\psi_z = -\pi/4$ radians compared to its pose in Graph A. In both scenario's $\kappa({}^{B}s_i)$ rates between 1.4 and 1.6 which means that a relative error of 1% in the position of the sensor in Frame B translates into a relative error in the range of 1.4–1.6% of the computed positions of the sensors in Frame C. This shows very good agreement with a previous error propagation analysis based on a 2D analysis [13]. For most of the planar space in Graphs A and B, $\kappa({}^{B}s_i)$ the relative error propagation exhibits a very small, seemingly linear increase with increasing distance to the lighthouse. The increase is minor however and supports the observation that the relative error propagation is nearly constant at a value just above 1.5 at a distance of more than 1 m. from the lighthouse. A nearly constant propagation of the relative error indicates that the absolute error in the position of ${}^{C}s$ is nearly proportional with the distance of ${}^{C}s$ to ${}^{C}0$. Closer to the lighthouse, $\kappa({}^{B}s_i)$ decreases as the difference between the sounding angles of the sensors become wider, which improves the conditioning of the position calculation, but at the same time makes the result more sensitive to the orientation of Frame B towards Frame C. This can be seen in Graph A at the higher z-side close to the lighthouse. Directly in front of the lighthouse, $\kappa({}^{B}s_i)$ has its minimum value, but if Frame B is moved sideways in either x-direction, $\kappa({}^{B}s_i)$ increases quite steeply as the consequence of the decreasing difference between the sounding angles of the sensors. This observation is supported by Graph B where Frame B is rotated. As a consequence the difference in sounding angles between the sensors now has its maximum off the origin of the x-axis, corresponding to the minimum value of $\kappa({}^{B}s_i)$ as reflected in the graph. These findings support the recommendation to equip a mobile frame to be operated in a lighthouse frame with more than 3 sensors, so that triplets of sensors with the largest difference in sounding angles can be selected to determine the vehicle's position. This is a subject for further study and optimization. The present analysis indicates that for the intended application here $\kappa({}^{B}s_i)$ rates between 1.4 and 1.6.

5. Measurement of the light sensor positions

To obtain the most accurate position for the light sensors with the minimum amount of effort, while avoiding use of expensive metrological equipment, the positions will be derived from simple length measurements. Length measurements are robust compared to most other measurements and require only simple tools and procedures. Since it is hard to measure distance to a light sensor as argued in Section 4, it will be performed by the light sensor itself, by turning Frame B around one fixed anchor point ${}^{C}p$ in Frame C on a flat surface. In Frame B the point of rotation is referred to as "swivel point", ${}^{B}p_j, j \in (1, 2, \ldots, m)$. For the purpose of locating sensor ${}^{B}s_i$, Frame B has multiple (m) swivel points. When swiveling Frame B around ${}^{B}p_j$, the swivel point (${}^{B}p_j$) is aligned with anchor point ${}^{C}p$ at the swivel axis, as shown in Fig. 5 for ${}^{B}p_1$. The light sensors are fixed on the mobile frame (Frame B). Frame B swivels around a fixed anchor point in Frame C. Consequentially the sensors rotate around the anchor point as well. Fig. 6 illustrates the circular paths ${}^{B}c_{i,j}$ and their radii $r_{i,j}$, $i \in (1, 2, \ldots, n)$, $j \in (1, 2, \ldots, m)$ traveled by sensor s_i in each swivel motion of the mobile frame around a different swivel point ${}^{B}p_j$. n is the number of light sensors of which at least three are required to establish the position of Frame B in Frame C as explained in Section 4: $n \geqslant 3$. The position of sensor s_i in Frame B occurs at the intersection of the circles and is determined unambiguously by the intersection of the paths around at least three different swivel points at known positions in Frame B: $m \geqslant 3$. As the different rotations of the mobile frame use the same fixed anchor point ${}^{C}p$, the circles described by light sensor s_i occur

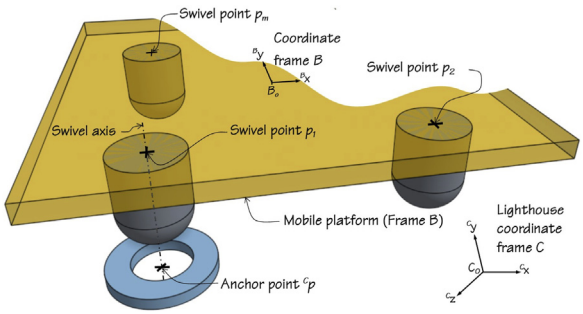

Fig. 5. Illustration of anchor point ${}^{C}p$, swivel points ${}^{B}p_j, j \in (1, 2, \ldots, m \geqslant 3)$ and the alignment of ${}^{C}p$ and ${}^{B}p_1$ at the swivel axis.

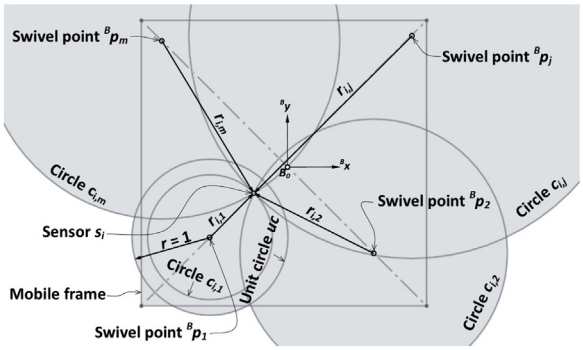

Fig. 6. Circular paths ${}^{B}c_{i,j}$ of sensor s_i around swivel points ${}^{B}p_j, j \in (1, 2, \ldots, m)$ in Frame B.

as concentric circles ${}^{C}c_{i,j}$ around ${}^{C}p$ in Frame C, as depicted in Fig. 7. In its recommended setup for the lighthouse, the angles at which s_i is sounded by the light sheets on its circular path ${}^{C}c_{i,j}$ around swivel point ${}^{B}p_j$, represent an ellipse ${}^{P}c_{i,j}$ in perspective projection plane P, as expressed by Eq. (1) and illustrated in Fig. 7 [14]. Using methods for camera calibration, geometrical parameters can be extracted from the image of each ellipse ${}^{P}c_{i,j}$ and applied to reconstruct the position of the center ${}^{C}ucc_{i,j}$ of a unit circle ${}^{C}uc_{i,j}$ with the same elliptic perspective projection ${}^{P}c_{i,j}$. Appendix B elaborates the method of Philip for the construction of the unit circle [15].

Fig. 7 shows corresponding sets of a unit circle ${}^{C}uc_{i,j}$ sharing the same perspective projection ${}^{P}c_{i,j}$ with circle ${}^{C}c_{i,j}$, drawn up by sensor s_i on its path around swivel point ${}^{B}p_j$. It can be observed in Fig. 7 that the distance $\|{}^{C}ucc_{i,j}\|$ from the lighthouse in ${}^{C}0 = {}^{C}[0\,0\,0]$ to ${}^{C}ucc_{i,j}$, is inversely proportional to radius $r_{i,j}$ of the corresponding circle ${}^{C}c_{i,j}$: $\|{}^{C}ucc_{i,j}\| \sim r_{i,j}^{-1}$. This allows for the definition of a ratio $\rho_{i,j}$ shown in Eq. (6), that expresses $r_{i,j}$ as a fraction of radius $r_{i,max}$ of circular path ${}^{C}c_{i,max}$, that is traveled by light sensor s_i around swivel point ${}^{B}p_{max}$ furthest away from s_i. Obviously ${}^{C}c_{i,max}$ is the circular path with largest radius $r_{i,max}$ of the paths traveled by s_i around all swivel points ${}^{B}p_j, j \in (1, 2, \ldots, m)$, $m \geqslant 3$. In Figs. 6 and 7, ${}^{C}c_{i,max}$ coincides with the circle indicated as ${}^{C}c_{i,j}$:

$$\rho_{i,j} = \frac{r_{i,j}}{r_{i,\max}} = \frac{\|{}^{C}ucc_{i,\max}\|}{\|{}^{C}ucc_{i,j}\|} \tag{6}$$

$$r_{i,\max} = \max(r_{i,j})$$
$$i \in (1, 2, \ldots, n)$$
$$j \in (1, 2, \ldots, m)$$
$$n \geqslant 3 \quad m \geqslant 3$$

With $\rho_{i,j}$, $r_{i,j}$ can be expressed as:

$$r_{i,j} = \rho_{i,j} \|{}^{B}p_{\max} - {}^{B}s_i\|$$

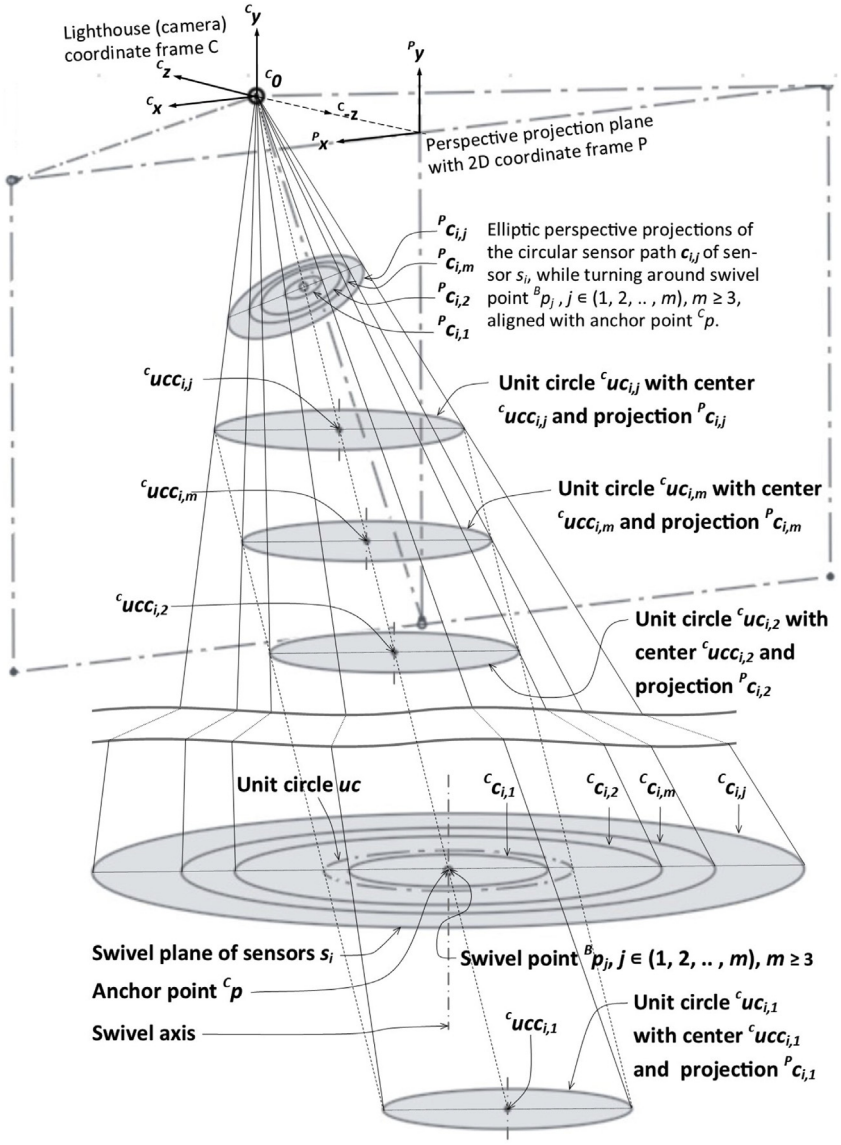

Fig. 7. Illustration of the circular paths of the swivel motion of light sensor s_i around anchor point ${}^C p$ in Frame C using different swivel points $p_j, j \in (1, 2, \ldots, m)$ and the unit circles sharing the same perspective projection.

The position of light sensor ${}^B s_i$ is at the intersection of circles ${}^B c_{i,j}$, $i \in (1, 2, \ldots, n)$, $n \geqslant 3$, in Frame B, for which an estimate ${}^{\tilde{B}} s_i$ can be found by the following minimization:

$$ {}^{\tilde{B}} s_i = \underset{{}^B s_i}{\operatorname{argmin}} \left[\sum_j \left(\| {}^B p_j - {}^B s_i \| - \rho_{i,j} \| {}^B p_{\max} - {}^B s_i \| \right)^2 \right] \tag{7} $$

The light sensor positions from the CAD file can serve here as a good starting point for the minimization.

6. Setup and experiments

6.1. Setup

To test the proposed approach to measure the light sensor positions, a mobile frame has been assembled sitting on legs with spherical caps at the bottom in each corner. The frame is shown in the top picture in Fig. 8. The mobile frame was designed to be 326 mm square, but came out of the industrial grade laser cutter with hand measurable deviations of up to 2 mm at the corners. This emphasizes the need for measurement of sensor positions even when using CAM parts. The legs under the frame act as swivel points in the experiments.

The accuracy of the positions of the legs in the assembled frame is critical to the accuracy of the position of the light sensors established in the experiments. Since these positions could deviate from their position in the CAD design as a consequence of the manufacturing tolerances observed, the mutual distance of the legs was measured and processed into positions using least square regression. The four legs acting as swivel points p_j, $j \in (1, 2, 3, 4)$ are numbered as indicated in Fig. 8 and have positions ${}^B p_j^T = [{}^B p x_j \; {}^B p y_j]$. There are $\binom{4}{2} = 6$ distances $d_{(j_1,j_2)}$ between each pair of legs $(p_{j_1}, p_{j_2}), (j_1, j_2) \in (1, 2, 3, 4), j_1 < j_2$, as listed in Table 1. To estimate the positions of the legs, three coordinates of the four legs have to be fixed to prevent kinematic solutions to occur: ${}^B p_1^T = [0\,0]$, ${}^B p y_4 = 0$.

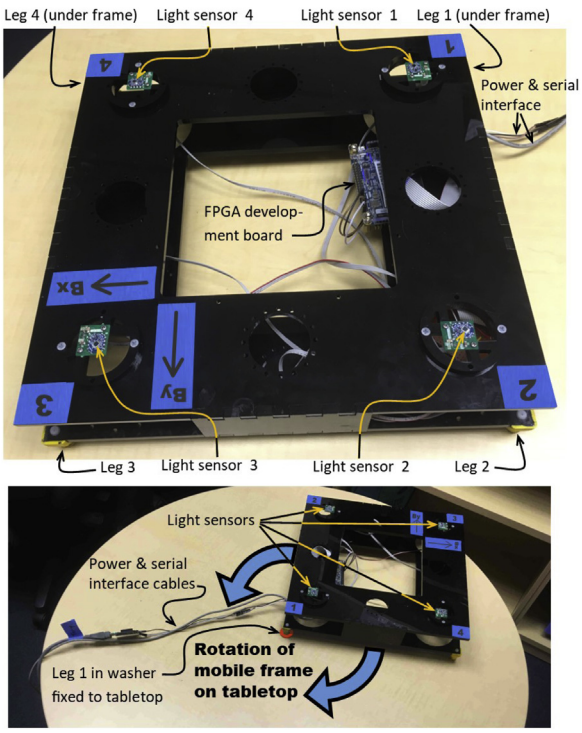

Fig. 8. Details of the mobile frame (top) and its operation on a tabletop (bottom).

Table 1
Positions of legs in the mobile frame.

Measured distances between leg i and leg j ($d_{(i,j)}$, [mm])					
$d_{(1,2)}=314$	$d_{(1,3)}=443$	$d_{(1,4)}=314$	$d_{(2,3)}=313.5$	$d_{(2,4)}=445$	$d_{(3,4)}=313.5$

CAD positions [mm]			Estimated positions [mm]		
Leg	${}^{B}x_l$	${}^{B}y_l$	Leg	${}^{B}x_l$	${}^{B}y_l$
l_1	0	0	l_1	0	0
l_2	0	314	l_2	– 0.9	314.1
l_3	314	314	l_3	312.7	313.6
l_4	314	0	l_4	314.1	0

Estimates for the remaining positions ${}^{\tilde{B}}p_j$, $j \in (2,3,4)$ can be found through:

$$ {}^{\tilde{B}}p_j = \underset{{}^{B}p_j}{\operatorname{argmin}} \left[\sum_{i,j} \left(\| {}^{B}p_{j_2} - {}^{B}l_{j_1} \| - \| d_{j_1,j_2} \| \right)^2 \right], \quad (j_1, j_2 \in (1,2,3,4),\ i<j) $$

The results of the estimate as listed in Table 1 will be used as the positions of the swivel points ${}^{B}p_j$ in the measurements of the light sensor positions.

For the actual position measurement with the lighthouse, the frame is equipped with four light sensors on top, designed to be at the same height, sharing the same plane in Frame B. The sensors share the same number with the leg it is closest to. The sensors comprise a BPW34S photo diode integrated in a Triad TS3633-CM1 "Light to Digital Converter" module, that are each connected to a digital input of a "DE0-Nano" development board. The signals of the sensors are identified by their port address. The development board carries an "Altera Cyclone IV" FPGA running at 50 MHz, allowing simultaneous detection of the edges generated by the passing of the light sheet over the light sensor, with a temporal resolution of 20 ns. The time stamps recorded by the FPGA are transmitted continuously through a serial connection over a USB port to a PC and stored for off-line processing.

6.2. Experiments

In the experiments, the mobile frame is moved over a table top as depicted in Fig. 8, with a lighthouse base station installed in a cabinet adjacent to the table, facing the frame. The lighthouse is positioned at about 40-60 cm vertical distance over the tabletop and at about 80–90 cm radial distance from the anchor point at the center of the table. The position of the lighthouse is given as a range as adjustments are made in between the experiments to prepare for the next run. In each run, the position of the lighthouse relative to the tabletop is fixed. The frame is rotated around one of its legs, turning in a washer as shown in Fig. 5, fixed in the center of the table top. The washer serves as the anchor point for the swivel motion. The spherical cap under the leg has a diameter slightly exceeding the inside diameter of the washer, creating a self-centering swivel of the cap in the washer. The frame is weighed with some ballast over the swivel point securing the leg in its centered position. To prevent the data communication over a cable connection between the FPGA board and connected PC to become entangled, the frame is pushed forth and backwards around the swivel point completing a full circle. This operation is repeated 10 times for all four legs, during which the time stamps are collected of the falling and rising edges of light pulses as explained in Section 2.

6.3. Results

The off-line post processing of the recorded time stamps starts with identification of the "heart beat" generated by the sync pulses of the lighthouse. These pulses are detected by multiple light sensors simultaneously and have the same duration on all sensors and a period of 8.333 ms, which makes them generally not hard to find. Once the heartbeat has been established identification of the light sheet and associated angle as well as calculation of the magnitude of the angle at which the light sensor is sounded is conducted according to the description in Section 2. "Graph A" in Fig. 9 illustrates the horizontal sounding angle (θ) for four sensors in one experiment. It can be observed that the range of sounding angles is smallest for sensor 4, indicating leg 4 was used as the swivel point in this experiment. Consequently sensor 2, located at the diagonal opposite side on the frame, swivels with the largest radius around leg 4, as reflected by the largest range in sounding angles: $r_{2,max} = r_{2,4}$. The periodicity of the graphs reveals the number of turns that the mobile frame has made (10) and the sample where the rotation was reversed, which is where the graphs of all light sensors have a local extreme simultaneously. The total number of (θ, ϕ) samples, N, taken for each sensor in an experiment comprising 10 turns of the mobile frame, is about $N = 10{,}000$. This implies that during each turn about 1000 soundings were taken, translating to a rotation angle of the frame of $2\pi/1000$ radians per sample. In the close up of the graph, depicted in "Graph B" the separate samples can be identified and the absence of visible noise in the sounding angles observed. This last finding concurs with the observation from Niehorster et al. that there is hardly jitter in the position measurements with the lighthouse system [7].

The image of the ellipse in "Graph C" is generated by plotting the tangent values of the measured data for θ and ϕ against each other for each combination of light sensor s_i and swivel point p_j. It is the result of the perspective projection of the circular paths of s_i around p_j, on perspective projection plane P. In the close up of the ellipses in "Graph D", it can be observed once more how clean the data is and how precise the samples of the 10 turns of the frame fit on top of each other. There is hardly any deviation between the 10 ellipses.

The obtained coordinate pairs: $[{}^{P}x_k \; {}^{P}y_k] = [\tan(\theta_k) \; \tan(\phi_k)]$ which each represent a point on the ellipse obtained from the measurement of θ_i and ϕ_i in sample interval k, $k \in (1, 2, \ldots, N)$, for each

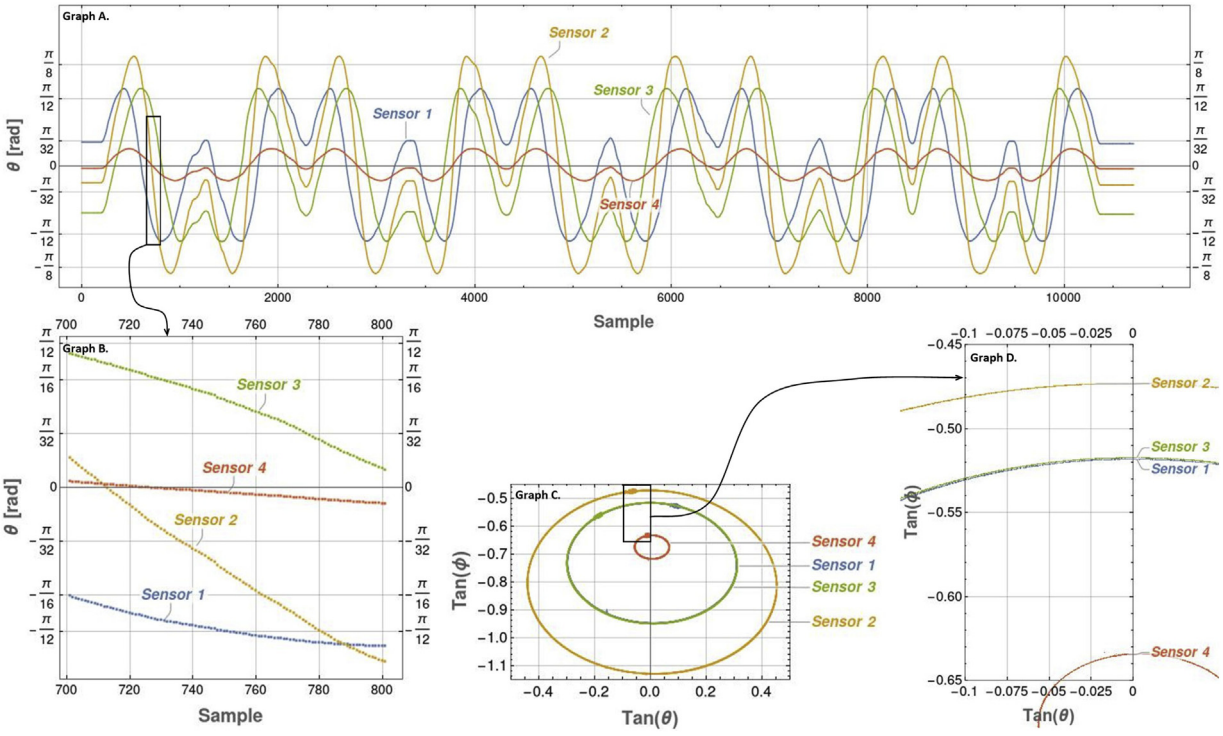

Fig. 9. Overview of the results from the swivel experiments using leg 4 of the mobile frame.

light sensor can now be used to compute the ellipse coefficients $(a_1, \ldots, a_6)$ in Eq. (B.2) in Appendix B:

$$Xa = 0 \tag{8}$$

where

$$X = \begin{bmatrix} {}^{P}x_1{}^2 & {}^{P}x_1{}^{P}y_1 & {}^{P}y_1{}^2 & {}^{P}x_1 & {}^{P}y_1 & 1 \\ & & \vdots & & & \\ {}^{P}x_N{}^2 & {}^{P}x_N{}^{P}y_N & {}^{P}y_N{}^2 & {}^{P}x_N & {}^{P}y_N & 1 \end{bmatrix}$$

and

$$a = \begin{bmatrix} a_1 & a_2 & a_3 & a_4 & a_5 & a_6 \end{bmatrix}$$

Since Eq. (8) is homogeneous in the coefficients a, the solution needs to be normalized to be unique: $||a|| = 1$. Under this constraint a can be solved by numerical minimization of $||Xa||$ [16]. Alternatively a fast solution can be obtained from the SVD of $X = U_X \Sigma_X V_X^T$, with U_X and V_X orthogonal matrices spanned by the left-singular and right-singular vectors of X. Σ_X is a diagonal matrix with the singular values $[\sigma_1 \ldots \sigma_m]$ of X, arranged in descending order. The SVD of X is applied as follows to minimize $||Xa||$:

$$\begin{aligned} \min_{\|a\|=1} \|Xa\| &= \min_{\|a\|=1} \|U_X \Sigma_X V_X^T a\| \\ &= \min_{\|a\|=1} \|U_X \Sigma_X (V_X^T a)\| = \min_{\|y\|=1} \|\Sigma_X y\| \\ &= \min_{\|y\|=1} (\sigma_1 y_1 + \cdots + \sigma_m y_m) \geq \sigma_m \end{aligned}$$

where $V_X^T a = y$. Hence, the minimum value for $||X\,a||$ is σ_m which will be attained for $y = [0\,0 \ldots 01]^T$. This implies that $a = V_X y = v_m$, the last right singular vector of X, corresponding to the smallest singular value [17].

With the ellipse coefficients $(a_1, \ldots, a_6)$, matrix Q can be assembled according to Eq. (B.4) and the position of the unit circle center ${}^{C}ucc_{i,j}$ determined following Expression (B.7) in Appendix B. The values obtained for ${}^{C}ucc_{i,j}$ allow for calculation of $\rho_{i,j}$ with Eq. (6) and subsequent solution of the light sensor position ${}^{B}s_i$ with Expression (7).

For the general case, where the light sensors are not swiveling in the same plane, Eq. (7) has to be solved for each sensor s_i separately, for all swivel points ${}^{B}p_j$, $j \in (1, 2, \ldots, m)$, $m \geqslant 3$. Since the light sensors in the present experiment are all mounted at the same height on top of the mobile frame and swivel in the same plane as a consequence, Expression (7) can be solved for all combinations of light sensors and swivel points simultaneously. The resulting sensor positions of this computation are listed in Table 2 together with the positions according to the CAD file.

7. Validation of the mobile frame path

The accuracy of the positions of the light sensors determined with the procedure described in Section 6, is investigated though reconstruction of the path of the mobile frame in the experiments and the path of the leg used as swivel point in particular. This leg only turns around its axis and does not translate in the experiments. Its stationary position in the turns with the mobile frame should be reflected in the reconstructed poses of the frame. In fact the deviation of the swivel point from its "mean" position in the reconstructed poses is not only a good measure for the precision of the lighthouse localization system but also of its accuracy as it is known that the true deviation is zero.

The path of Frame B in Frame C is simulated by reconstruction of the pose of the mobile frame for each sweep k of the lighthouse according to the procedure described in Section 4:

- Firstly the angles ${}^{C}\psi$ and position ${}^{C}B_0$ of Frame B in Frame C are estimated for all possible triplet combinations out of the available set of light sensors. Out of the positions calculated for each of these triplets a trimmed mean position ${}^{C}p_j(n)$ is established in which the triplet positions with the largest deviation to the calculated mean position are dropped. In this case with time stamps of four light sensors available, the worst 25% positions (being 1 position out of four triplets) is dropped.

Table 2
Measured ratio of sensor circle radii and sensor positions calculated from measurements and design (CAD) specifications.

Leg	Radii ratio, $rr_{i,j}$			Measured position [m]		CAD position [m]	
	1	2	4	${}^{B}x_i$	${}^{B}y_i$	${}^{B}x_i$	${}^{B}y_i$
Sensor 1	0.1514	0.7143	0.7127	−0.115073	−0.115619	−0.115375	−0.114918
Sensor 2	0.7154	0.1503	1	−0.116556	0.115984	−0.115375	0.116082
Sensor 3	1	0.7131	0.7158	0.115112	0.116721	0.115625	0.116082
Sensor 4	0.7157	1	0.1515	0.116342	−0.115441	0.115625	−0.114918

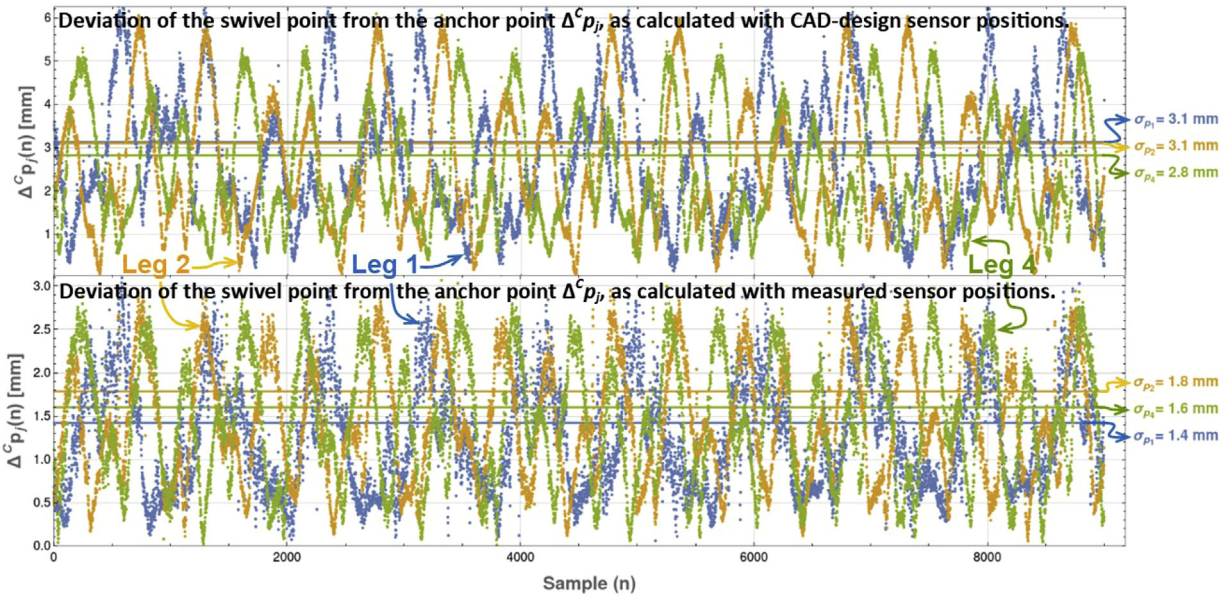

Fig. 10. Deviation of the calculated swivel point from the stationary anchor point in the swivel experiments.

Table 3
Comparison of the deviation of the reconstructed position of the swivel point for the light sensors in measured and design (CAD) position. All positions and standard deviations in meter.

Swivel point	Estimated position of anchor point: ${}^{\tilde{C}}p = {}^{C}\bar{p}_j$				Sensors in measured position		Sensors in CAD position	
j	${}^{c}x$	${}^{c}y$	${}^{c}z$	$\|{}^{\tilde{C}}p\|$	σ_{p_j}	$\sigma_{p_j}/\|{}^{\tilde{C}}p\|$	σ_{p_j}	$\sigma_{p_j}/\|{}^{\tilde{C}}p\|$
1	0.01034	−0.6398	0.9489	1.1445	0.001425	0.12%	0.003138	0.28%
2	−0.0355	−0.3859	0.7723	0.8641	0.001789	0.21%	0.003109	0.36%
4	−0.0356	−0.3849	0.7723	0.8637	0.001605	0.19%	0.002827	0.33%

- Then, applying the coordinate transformation of Eq. (2), using the value for ${}^{C}\psi$ and ${}^{C}B_0$ obtained in the previous step, the position of the swivel point p_j in Frame C is found by: ${}^{C}p_j = [R|T]\,{}^{B}p_j$, where $j \in (1, 2, 4)$ is the number of the leg used as swivel point.

The movement of the swivel point ${}^{C}p_j$ is expressed as the standard deviation σ_{p_j} of all positions sampled in an experiment with swivel point $j \in (1, 2, 4)$, comprising of about $N = 10{,}000$ samples:

$$
\begin{aligned}
{}^{C}\bar{p}_j &= \frac{1}{N}\sum_{n=1}^{N} {}^{C}p_j(n) \\
\Delta^{C}p_j(n) &= \|{}^{C}p_j(n) - {}^{C}\bar{p}_j\| \\
\sigma_{p_j} &= \sqrt{\frac{1}{N}\sum_{n=1}^{N} \Delta^{C}p_j(n)^2}
\end{aligned}
$$

$\Delta^{C}p_j(n)$ is plotted in Fig. 10 for the three swivel experiments with legs 1, 2 and 4, for the two cases simulated: with light sensors in design position according to the CAD file and with sensors in the measured positions. Table 3 summarizes the results. The position error of the swivel point is expressed as a relative error $\sigma_{p_j}/\|{}^{\tilde{C}}p\|$ which makes it independent of the distance from the light sensors to the lighthouse. This allows for easier comparison of the different results.

It can be observed that the improvement of the accuracy of the measurement of the light sensor positions has reduced σ_{p_j} by 40%, which is a significant increase of the precision of the localization of a mobile frame with a lighthouse system. Since it is known that the position of the anchor point is stationary in the swivel motion, the measured improvement of the precision of the position of Frame B in Frame C for different poses of Frame B, also expresses improvement of the accuracy of the position established with the lighthouse system. This is demonstrated by the graphs in Fig. 10 that exhibit periodicity of $\Delta^{C}p_j(n)$, in synchronization with the turns of the mobile frame. The periodicity reveals a systematic error in the localization of the anchor point, dominating the magnitude of $\Delta^{C}p_j(n)$, that is most likely caused by remaining inaccuracies of the positions of light sensors and swivel points. Hence $\Delta^{C}p_j(n)$ can be used as a cost function to identify and further minimize systematic errors in the localization with a lighthouse system.

The result of the present research to measure the positions of the light sensors on the mobile frame, is a reduction of the relative localization error of the lighthouse system from over 0.3% to below 0.2% using one lighthouse base station.

8. Conclusions and future work

The findings in the present paper can be summarized in the following conclusions:

- The relative condition number for the propagation of errors in the position of light sensor into the calculated position of a mobile frame rates between 1.4 and 1.6 for the HTC Vive lighthouse system base station.
- The nearly constant value of relative condition number over most of the operating range of the lighthouse implies that the error in the calculated position of a mobile frame is about linear with the distance to the lighthouse base-station.
- The procedure presented to create circular features in the projection image of a lighthouse system is easy to execute and allows available camera calibration techniques to be applied directly to measure light sensor position on a mobile frame for use with the lighthouse system.
- Camera calibration techniques are an effective way to improve the accuracy of the position measurement without using external measurement instruments.
- After measuring the light sensor positions on the experimental mobile frame with the present procedure, the relative error of the position of the mobile frame established with one lighthouse base station, dropped from over 0.3% to below 0.2% (meter error per meter distance).

The research has identified and opened up many opportunities for future work.

- Derivation of a relative condition number for the propagation of errors in the sounding angle of light sensors into the calculated position of the mobile frame.
- The position of the lighthouse itself is a factor of relevance. For tracking of motions in a planar space the best position of the lighthouse could be overhead of the plane.
- The model presented is purely static and is sufficient for the measurement of light sensor positions. It can be extended to a dynamic model with real time updates of the position of all sensors with techniques such as Kalman filtering for localization of the mobile frame in motion
- The analysis in Section 4 shows some dependency of the error propagation from the pose of the mobile frame which opens up opportunities to optimize placement of light sensors and/or choose subsets of the sensors with the best conditioning for low error propagation depending in the pose of the frame.
- Analysis of the combination of multiple lighthouse base stations is likely the strongest approach towards improved accuracy of the localization accuracy, but will come with increased complexity.

Authors' contribution

A.F.M. Paijens: conceptualization, methodology, firmware development, experiments, writing, editing. L. Huang: principal-supervision, conceptualization, methodology, reviewing, editing correspondence. A.M. Al-Jumaily: co-supervision, conceptualization, reviewing.

Declaration of Competing Interest

The authors report no declarations of interest.

Acknowledgment

The authors want to thank John Collins and Jian Huang from Auckland University of Technology for their support to the preparation, execution and processing of the experiments.

Appendix A. Elaboration of the Jacobian $J({}^{C}s, {}^{B}s)$

For all expressions applies that the index i refers to any triplet of three light sensors s_j, s_k and s_l of all available sensors. A triplet is the minimum of three light sensors that is required to obtain a position of Frame B in Frame C. It implies that the Jacobian $\partial {}^{C}s_i/\partial {}^{B}s_i$ has $9 \times 9 = 81$ elements. Plugging the expressions for ${}^{P}s_i$ from Eq. (1) in Eq. (5) yields:

$$\frac{\partial {}^{P}s_i^T}{\partial {}^{C}Bs_i} = \left[\frac{\partial({}^{C}x_i/{}^{C}z_i)}{\partial {}^{B}s_i} \frac{\partial({}^{C}y_i/{}^{C}z_i)}{\partial {}^{B}s_i} \right] = [0\ 0] \tag{A.1}$$

Application of the chain rule for differentiation expands the elements in vector $\partial {}^{P}s_i^T/\partial {}^{C}Bs_i$ as shown here for the first element ${}^{P}x_i = {}^{C}x_i/{}^{C}z_i$:

$$\frac{\partial({}^{C}x_i/{}^{C}z_i)}{\partial {}^{B}s} = \left({}^{C}z_i \frac{\partial {}^{C}x_i}{\partial {}^{B}s} - {}^{C}x_i \frac{\partial {}^{C}z_i}{\partial {}^{B}s} \right) \frac{1}{{}^{C}z_i^2} \tag{A.2}$$

Since the z-coordinate ${}^{C}z_i$ of any light sensor on the mobile frame will never be zero in the lighthouse coordinate system, Eq. (A.1) can be solved by finding the roots of the numerator in Eq. (A.2):

$${}^{C}z_i \left(\frac{\partial {}^{C}x_i}{\partial {}^{B}s} \right) - {}^{C}x_i \left(\frac{\partial {}^{C}z_i}{\partial {}^{B}s} \right) = 0 \tag{A.3}$$

The two terms of this equation can be elaborated further by plugging into Eq. (A.3), the transformation of ${}^{B}s_i$ into ${}^{C}s_i$ according to Eq. (2):

$${}^{C}s_i = \left[R({}^{C}\psi({}^{B}s)) | T({}^{C}B_0({}^{B}s)) \right] \left[{}^{B}s_i | 1 \right]^T$$

For compactness of writing, the transformation matrix $\left[R({}^{C}\psi({}^{B}s)) | T({}^{C}B_0({}^{B}s)) \right]$ will be further referred to as TR. The rows in this transformation matrix will be identified by a subscript, hence:

$${}^{C}x_i = TR_1 \left[{}^{B}s_i | 1 \right]^T \tag{A.4}$$

Differentiating Eq. (A.4) to ${}^{B}s$ yields:

$$\begin{aligned} \frac{\partial {}^{C}x_i}{\partial {}^{B}s} = \left[{}^{B}s_i | 1 \right] & \left[\frac{\partial TR_1}{\partial {}^{C}\psi} | \frac{\partial TR_1}{\partial {}^{C}B_0} \right] \begin{bmatrix} \frac{\partial {}^{C}\psi}{\partial {}^{B}s} \\ \frac{\partial {}^{C}B_0}{\partial {}^{B}s} \end{bmatrix} \\ & + TR_1 \frac{d}{d{}^{B}s} \begin{bmatrix} {}^{B}s_i \\ 1 \end{bmatrix} \end{aligned} \tag{A.5}$$

Plugging Eq. (A.5) into (A.3), together with the equivalent expression for $\partial {}^{C}z_i/\partial {}^{B}s$, the following relationship is obtained for $\partial({}^{C}x_i/{}^{C}z_i)/\partial {}^{B}s$:

$$\begin{aligned} & \frac{\partial({}^{C}x_i/{}^{C}z_i)}{\partial {}^{B}s} = \\ & \left[{}^{B}s_i | 1 \right] \left({}^{C}z_i \left[\frac{\partial TR_1}{\partial {}^{C}\psi} | \frac{\partial TR_1}{\partial {}^{C}B_0} \right] - {}^{C}x_i \left[\frac{\partial TR_3}{\partial {}^{C}\psi} | \frac{\partial TR_3}{\partial {}^{C}B_0} \right] \right) \begin{bmatrix} \frac{\partial {}^{C}\psi}{\partial {}^{B}s} \\ \frac{\partial {}^{C}b_0}{\partial {}^{B}s} \end{bmatrix} \\ & + \left({}^{C}z_i TR_1 - {}^{C}x_i TR_3 \right) \frac{d}{d{}^{B}s} \begin{bmatrix} {}^{B}s_i \\ 1 \end{bmatrix} \end{aligned} \tag{A.6}$$

An equation similar to Eq. (A.6) can be formulated for $\partial({}^{C}y_i/{}^{C}z_i)/\partial\,{}^{B}s$ by substitution of ${}^{C}y_i$ and TR_2 for ${}^{C}x_i$ and TR_1, respectively. For the three light sensors used to locate the mobile frame in the lighthouse coordinate system this provides three pairs of equations spanning a system of linear equations of the form:

$$A\begin{bmatrix}\frac{\partial\,{}^{C}\psi}{\partial\,{}^{B}s}\\ \frac{\partial\,{}^{C}B_0}{\partial\,{}^{B}s}\end{bmatrix} = b \tag{A.7}$$

with

$$A = \begin{bmatrix} \begin{bmatrix}{}^{B}s_1|1\end{bmatrix}\left({}^{C}z_1\begin{bmatrix}\frac{\partial TR_1}{\partial\,{}^{C}\psi}|\frac{\partial TR_1}{\partial\,{}^{C}B_0}\end{bmatrix} - {}^{C}x_1\begin{bmatrix}\frac{\partial TR_3}{\partial\,{}^{C}\psi}|\frac{\partial TR_3}{\partial\,{}^{C}B_0}\end{bmatrix}\right)\\ \begin{bmatrix}{}^{B}s_1|1\end{bmatrix}\left({}^{C}z_1\begin{bmatrix}\frac{\partial TR_2}{\partial\,{}^{C}\psi}|\frac{\partial TR_2}{\partial\,{}^{C}B_0}\end{bmatrix} - {}^{C}y_1\begin{bmatrix}\frac{\partial TR_3}{\partial\,{}^{C}\psi}|\frac{\partial TR_3}{\partial\,{}^{C}B_0}\end{bmatrix}\right)\\ \vdots\\ \begin{bmatrix}{}^{B}s_3|1\end{bmatrix}\left({}^{C}z_3\begin{bmatrix}\frac{\partial TR_2}{\partial\,{}^{C}\psi}|\frac{\partial TR_2}{\partial\,{}^{C}B_0}\end{bmatrix} - {}^{C}y_3\begin{bmatrix}\frac{\partial TR_3}{\partial\,{}^{C}\psi}|\frac{\partial TR_3}{\partial\,{}^{C}B_0}\end{bmatrix}\right)\end{bmatrix}$$

and

$$b = \begin{bmatrix}\left({}^{C}x_1\,TR_3 - {}^{C}z_1\,TR_1\right)\frac{d}{d^{B}s}\begin{bmatrix}{}^{B}s_1\\1\end{bmatrix}\\ \left({}^{C}y_1\,TR_3 - {}^{C}z_1\,TR_2\right)\frac{d}{d^{B}s}\begin{bmatrix}{}^{B}s_1\\1\end{bmatrix}\\ \vdots\\ \left({}^{C}y_3\,TR_3 - {}^{C}z_3\,TR_2\right)\frac{d}{d^{B}s}\begin{bmatrix}{}^{B}s_3\\1\end{bmatrix}\end{bmatrix} \tag{A.8}$$

Using the Mathematica function "LinearSolve" the 27 elements of each of the Jacobian matrices $\partial\,{}^{C}\psi/\partial\,{}^{B}s$ and $\partial\,{}^{C}B_0/\partial\,{}^{B}s$ are computed by solving Eq. (A.7). Plugging the resulting matrices into Eq. (4) completes the calculation of $J({}^{C}s, {}^{B}s)$ as shown in Fig. 4.

Appendix B. Determinating the position of a unit circle in 3D from its 2D perspective projection

Camera projections of circular features have been researched extensively to develop methods to reconstruct the position and orientation of circles relative to the camera. The approach by Philip [15] starts with the parametric definition of the points ${}^{C}uc_k$ on a unit circle ${}^{C}uc$ in the camera space, Frame C:

$$\begin{aligned}{}^{C}uc_k &= [{}^{C}x_k\ {}^{C}y_k\ {}^{C}z_k]^T\\ &= {}^{C}ucc + {}^{C}e_1\cos(\xi_k) + {}^{C}e_2\sin(\xi_k)\\ &\quad k \in (1,2,\ldots,l),\quad 0 \leqslant \xi_k \leqslant 2\pi\end{aligned} \tag{B.1}$$

Angle ξ_k is the parameter indicating the position of point ${}^{C}uc_k$ in polar notation. ${}^{C}ucc$ is the circle center and ${}^{C}e_1$ and ${}^{C}e_2$ are orthogonal unit vectors spanning the circle plane in Frame C. As the consequence of the perspective projection, this circle will be recorded as an ellipse on the projection plane P as illustrated in Fig. B.11.

Points ${}^{P}c_k = [{}^{P}x_k\ {}^{P}y_k]^T$ on the same ellipse in the projection plane have the following relationship:

$$a_1\,{}^{C}Px_k^2 + a_2\,{}^{C}Px_k\,{}^{C}Py_k + a_3\,{}^{C}Py_k^2 + a_4\,{}^{C}Px_k + a_5\,{}^{C}Py_k + a_6 = 0 \tag{B.2}$$

Inserting the expression for perspective projection from Eq. (1) in Eq. (B.2), the ellipse can be formulated in matrix form in coordinates of Frame C, as:

$${}^{C}c_k\,{}^{C}TQ\,{}^{C}c_k = 0 \tag{B.3}$$

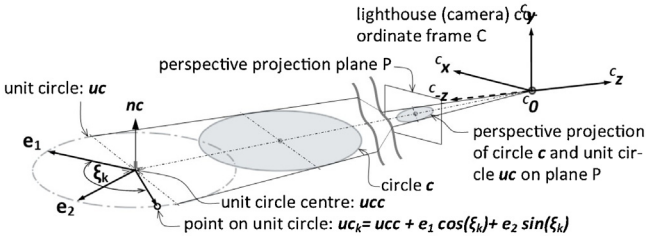

Fig. B.11. Reconstruction of the position of a unit circle from its elliptic perspective projection.

where

$$Q = \frac{1}{2}\begin{bmatrix}2a_1 & a_2 & a_4\\ a_2 & 2a_3 & a_5\\ a_4 & a_5 & 2a_6\end{bmatrix}$$

Matrix Q can be scaled as appropriate, as Eq. (B.3) is homogeneous. Since Q is a symmetrical matrix with real elements it can be replaced with its eigenvalue decomposition:

$$Q = V_Q\,\Lambda_Q\,V_Q^T \tag{B.4}$$

in which V_Q is an orthonormal (rotation) matrix and Λ_Q is the diagonal matrix with eigenvalues λ_1, λ_2 and λ_3 of Q: $\Lambda_Q = \mathrm{diag}[\lambda_1\ \lambda_2\ \lambda_3]$, $\lambda_1 \geqslant \lambda_2 > 0 > \lambda_3$.

Inserting Eqs. (B.4) and (B.1) in Eq. (B.3), while substituting $\Pi = V_Q^T\,{}^{C}ucc, f_1 = V_Q^T\,{}^{C}e_1$ and $f_2 = V_Q^T\,{}^{C}e_2$ the following conditions can be extracted that have to be met in order for Eq. (B.3) to be true for all ξ_k:

$$f_1^T\Lambda_Q f_1 = f_2^T\Lambda_Q f_2 = \Pi^T\Lambda_Q\Pi \tag{B.5}$$

$$f_1^T\Lambda_Q f_2 = \Pi^T\Lambda_Q f_1 = \Pi^T\Lambda_Q f_2 = 0 \tag{B.6}$$

Conditions (B.5) and (B.6) don't fully define Π, f_1 and f_2, as the circle can be rotated in the circle plane around ${}^{C}ucc$, without changing the circle definition. f_1 and f_2 can therefore be freely chosen in the circle plane within the constraint that they have to be orthogonal. Philip proposes to use [15]:

$$f_1 = \frac{1}{\sqrt{2}}[\cos(\varphi)\ 1\ \ \sin(\varphi)]^T$$

$$f_2 = \frac{1}{\sqrt{2}}[-\cos(\varphi)\ 1\ \ -\sin(\varphi)]^T$$

which meets the conditions for f_1 and f_2 in Eq. (B.5). Angular parameter φ is determined by Eq. (B.6):

$$\cos(\varphi)^2 = \frac{\lambda_2 - \lambda_3}{\lambda_1 - \lambda_3}$$

This establishes the normal vector ${}^{C}nc$ of the circle and unit circle plane:

$${}^{C}nc = {}^{C}e_1 \times {}^{C}e_2 = \pm V_Q(f_1 \times f_2) = \pm V_Q[-\sin(\varphi)\ 0\ \ \cos(\varphi)]^T$$

Π can be determined from the condition of Eq. (B.6) that it is orthogonal to f_1 and f_2:

$$\Pi = c_\Pi(f_1 \times f_2) = c_\Pi\lambda_2[-\lambda_3\sin(\varphi)\ 0\ \lambda_2\cos(\varphi)]^T$$

Constant c_Π can be derived from the conditions imposed by Eq. (B.6). With Π resolved, the position of the circle center ${}^{C}ucc$, can be expressed as:

$${}^{C}ucc = V\Pi = \pm V_Q\left[-\sqrt{\frac{-\lambda_3}{\lambda_1}}\sin(\varphi)\ 0\ \sqrt{\frac{-\lambda_1}{\lambda_3}}\cos(\varphi)\right]^T \tag{B.7}$$

The sign for V_Q in Eq. (B.7) is easily recognized through comparison of the calculation of ${}^{C}ucc$ with the position of the anchor point in the physical setup. This completes the computation of the center and orientation of the unit circle according to Philip [15].

References

[1] T. Tsumura, N. Fujiwara, M. Hashimoto, T. Tang, A new method of vehicle position and heading measurement by use of a laser-beacon, J. Robot. Soc. Jpn. 2 (6) (1984) 557–565.

[2] S. Hernández, J. Torres, C. Morales, L. Acosta, A new low cost system for autonomous robot heading and position localization in a closed area, Auton. Robots 15 (2) (2003) 99–110, http://dx.doi.org/10.1023/a:1025550223554.

[3] S. Islam, B. Ionescu, C. Gadea, D. Ionescu, Indoor positional tracking using dual-axis rotating laser sweeps, 2016 IEEE International Instrumentation and Measurement Technology Conference Proceedings (2016) 1–6, http://dx.doi.org/10.1109/i2mtc.2016.7520559.

[4] A. Paijens, L. Huang, A. Al-Jumaily, Mobile robot positioning system for precision manufacturing: the laser lighthouse revisited, 2017 3rd International Conference on Control, Automation and Robotics (ICCAR) (2017), http://dx.doi.org/10.1109/iccar.2017.7942666.

[5] M. Greiff, A. Robertsson, K. Berntorp, Performance bounds in positioning with the vive lighthouse system, 2019 22th International Conference on Information Fusion (FUSION) (2019) 1–8.

[6] B. Kilberg, F. Campos, F. Maksimovic, T. Watteyne, K. Pister, Accurate 3d lighthouse localization of a low-power crystal-free single-chip mote, J. Microelectromech. Syst. 29 (2020) 818–824, http://dx.doi.org/10.1109/jmems.2020.3011460.

[7] D.C. Niehorster, L. Li, M. Lappe, The accuracy and precision of position and orientation tracking in the htc vive virtual reality system for scientific research, i-Perception 8 (3) (2017), http://dx.doi.org/10.1177/2041669517708205, 2041669517708205.

[8] W. Jansen, D. Laurijssen, W. Daems, J. Steckel, Automatic calibration of a six-degrees-of-freedom pose estimation system, IEEE Sens. J. 19 (2019) 8824–8831, http://dx.doi.org/10.1109/JSEN.2019.2921644.

[9] K. Sletten, Automated Testing of Industrial Robots Using htc Vive for Motion Tracking, University of Stavanger, Norway, 2017 (Master's thesis).

[10] M. Borges, A. Symington, B. Coltin, T. Smith, R. Ventura, HTC vive: analysis and accuracy improvement, 2018 IEEE/RSJ International Conference on Intelligent Robots and Systems (IROS) (2018), http://dx.doi.org/10.1109/iros.2018.8593707.

[11] L. Trefethen, D. Bau, Numerical Linear Algebra, Other Titles in Applied Mathematics, Society for Industrial and Applied Mathematics (SIAM), 1997.

[12] A. Ranganathan, The Levenberg–Marquardt Algorithm, Lecture Notes, Georgia Institute of Technology, Georgia, USA, 2004 June.

[13] A. Paijens, L. Huang, A. Al-Jumaily, Analysis of sensor arrangements to localize mobile robots with one laser lighthouse, 2017 24th International Conference on Mechatronics and Machine Vision in Practice (M2VIP) (2017), http://dx.doi.org/10.1109/m2vip.2017.8211469.

[14] D. Salomon, The Computer Graphics Manual, Texts in Computer Science, Springer London, 2011.

[15] J. Philip, An Algorithm for Determining the Position of a Circle in 3D From Its Perspective 2D Projection, Department of Mathematics, Royal Institute of Technology, 1997.

[16] A. Fitzgibbon, M. Pilu, R. Fisher, Direct least square fitting of ellipses, IEEE Trans. Pattern Anal. Mach. Intell. 21 (5) (1999) 476–480, http://dx.doi.org/10.1109/34.765658.

[17] W. Gander, The Singular Value Decomposition, Lecture Notes, ETH Zurich, 2008.

Biographies

Tony Paijens graduated with a Master degree in Mechanical Engineering from Delft University of Technology (TU-Delft) in the Netherlands in 1987. He worked as a process engineer at Akzo Nobel from 1987 to 1990, after which he lectured at TU-Delft from 1990 to 2006. Subsequently he ventured into entrepreneurship in the design, construction and operation of supercritical extraction plants in South East Asia over a period of eight years. Presently he pursues his PhD at Auckland University of Technology. His interest are in robotic technologies for manufacturing.

Loulin Huang is an associate professor in Mechatronics in Auckland University of Technology (AUT). He had about thirty years' research experience in the areas of robotics, mechatronics and control in his academic careers in Huazhong University of Science and Technology (China), Singapore Polytechnic (Singapore), Massey University (New Zealand) and AUT. He has completed more than thirty industrial and government-funded projects in robotics and mechatronics, and published about ninety papers and two books. The systems developed from his projects include international award winning mobile robot systems for soccer games which have been adopted by the institutions in Singapore, India, China, New Zealand and Hong Kong, and the automatic road texture depth monitoring system which has been used in the road projects in New Zealand and Australia.

Ahmed Al-Jumaily is currently a Professor of Biomechanical Engineering at the Institute of Biomedical Technologies at the Auckland University of Technology, New Zealand. He is a member of 11 international professional societies. He is the Editor-in-Chief of the ASME Journal of Engineering and Science in Medical Diagnostics and Therapy and of the ASME monograph series-Biomedical and Nanomedical Technologies. Published more than 350 papers in international journals and conference proceedings in Biomedical applications, system dynamics, vibrations and control.